A Multi-material Low Phase Noise Optomechanical Oscillator

Turker Beyazoglu

Electrical Engineering and Computer Sciences
University of California at Berkeley

Technical Report No. UCB/EECS-2014-235
http://www.eecs.berkeley.edu/Pubs/TechRpts/2014/EECS-2014-235.html

December 19, 2014

A Multi-material Low Phase Noise Optomechanical Oscillator

by

Turker Beyazoglu

A report submitted in partial satisfaction of the

requirements for the degree of

Master of Science

in

Engineering – Electrical Engineering and Computer Sciences

in the

Graduate Division

of the

University of California, Berkeley

Committee in charge:

Professor Clark T.-C. Nguyen, Chair

Professor Ming C. Wu

Fall 2014

A Multi-material Low Phase Noise Optomechanical Oscillator

A Multi-material Low Phase Noise Optomechanical Oscillator

by

Turker Beyazoglu

Research Project

Submitted to the Department of Electrical Engineering and Computer Sciences, University of California at Berkeley, in partial satisfaction of the requirements for the degree of **Master of Science, Plan II**.

Approval for the Report and Comprehensive Examination:

Committee:

Professor Clark T.-C. Nguyen
Research Advisor

(Date)

* * * * * * *

Professor Ming C. Wu
Second Reader

(Date)

A Multi-material Low Phase Noise Optomechanical Oscillator

by

Turker Beyazoglu

Master of Science in Electrical Engineering and Computer Sciences

University of California, Berkeley

Professor Clark T.-C. Nguyen, Chair

Recent advancements in cavity optomechanics have allowed researchers to exploit coupling between the optical field and mechanical motion of an optical cavity to affect cooling or amplification of mechanical motion. Cooling the mechanical motion of microscale objects has been of high scientific interest, since it facilitates observation and exploration of certain quantum phenomena, e.g., the standard quantum limit of detection. On the other hand, amplification of the mechanical motion allows realization of microscale devices for practical applications, such as light driven low phase noise signal generation by Radiation Pressure driven OptoMechanical Oscillators (RP-OMO).

The ability to achieve self-sustained oscillation with no need for feedback electronics makes an RP-OMO compelling for on-chip applications where directed light energy, e.g., from a laser, is available to fuel the oscillation, such as Chip Scale Atomic Clocks (CSAC). Indeed, an RP-OMO can substantially reduce power consumption of a CSAC by replacing its power-hungry conventional quartz-based microwave synthesizer but this requires that the RP-OMO output be sufficiently stable, as gauged over short time spans by its phase noise. This motivates a focus on achieving a high mechanical Q (Q_m) RP-OMO to have low phase noise while maintaining a reasonably high optical Q (Q_o) for low power operation—a challenge in previous OMOs that had to trade-off Q_m and Q_m mainly because they use a single material to set both its Q_m and Q_o.

The work in this report presents a multi-material RP-OMO that circumvents this limitation by combining a silicon nitride optical material with a lower mechanical loss polysilicon material to attain simultaneous high Q_m and Q_o. The multi-material RP-OMO structure boosts the Q_m of a silicon nitride RP-OMO by more than 2× toward realization of the simultaneous high Q_m >22,000 and Q_o >190,000 needed to maximize RP-OMO performance. With its high Q_m, the multi-material RP-OMO exhibits a best-to-date phase noise of -114 dBc/Hz at 1 kHz offset from its 52-MHz carrier—a 12 dB improvement from the previous best by an RP-OMO constructed of silicon nitride alone. The doped polysilicon structure and electrodes additionally allow tuning of the RP-OMO's oscillation frequency via DC voltage, enabling future deployment of the multi-material RP-OMO as a locked oscillator in a target low-power CSAC application.

Table of Contents

List of Figures

List of Tables

Acknowledgments

I would like to express my gratitude to my advisor Professor Clark Nguyen for his support, guidance, and providing me with a great environment for doing research. I would also like to thank Professor Ming Wu for his support and providing an excellent opportunity to collaborate with his group.

I am also grateful to my colleagues Alejandro Grine, Karen Grutter, Niels Quack, and Tristan Rocheleau, who worked with me on different aspects of this work. Our collaboration has always been very fruitful and I have learned a lot from them. It has always been a pleasure to work with the Nguyen research group members Mehmet Akgul, Henry Barrow, Li-Wen Hung, Divya Kashyap, Wei-Chang Li, Yang Lin, Ruonan Liu, Thura Lin Naing, Jalal Naghsh Nilchi, Alper Ozgurluk, Brian Pepin, Zeying Ren, Tommi Riekkinen and Robert Schneider.

I appreciate the help from the Marvell Nanofabrication Laboratory staff who do their best to maintain a good lab and respond to everyone's needs.

Finally, I would like to express my deepest gratitude to my family. I cannot thank you enough for your constant, unconditional love and support.

Chapter 1

Introduction and Overview

1.1 Radiation Pressure Driven Optomechanical Oscillators

Photons, just like any other particle, carry momentum. A photon reflecting from a surface imparts a pressure due to the transfer of momentum, generally referred to as radiation pressure. When light is confined in a high quality factor optical cavity, the optical field builds up to a sizable optical power so the radiation pressure becomes large enough to observe deformation on the optical cavity. The coupling of optical and mechanical degrees-of-freedom by the radiation pressure has led to observation of regenerative mechanical oscillations in micro-cavities and a new class of microwave oscillators has emerged which harness light power to sustain the oscillation.

A Radiation Pressure driven OptoMechanical Oscillator (RP-OMO) generally consists of a micro-ring, toroid or disk shaped device that acts simultaneously as an optical and a mechanical resonator. Typically, the optical resonance in these devices is a Whispering Gallery Mode (WGM) while the mechanical resonance is the radial contour (breathing) mode. There are also slot-type OMOs that use a photonic crystal design to guide the optical mode in doubly-clamped nanobeams vibrating in-plane. When blue-detuned laser light couples into the RP-OMO, radiation pressure force can drive it into mechanical oscillation if the laser power is sufficient to sustain the oscillation. The oscillating RP-OMO motion results in modulation of the optical field amplitude at the mechanical oscillation frequency which can be demodulated by a photodiode to isolate the mechanical oscillation. The nonlinear optomechanical transduction within the RP-OMO also enables generation of frequency combs occurring at the harmonics of the mechanical frequency.

1.2 Previous Work

To date, RP-OMOs have found applications in microwave frequency generation [1], communications [2], and sensing [3]. To be useful in such applications, the output of an RP-OMO must be sufficiently stable, as gauged over short time spans by its phase noise. This section gives a brief review of previous work with the emphasis on phase noise performance and required optical threshold power (P_{th}) to obtain oscillation. It is also important to note the values of the mechanical Q (Q_m) and the optical Q (Q_o) since they ultimately govern these performances to a great extent, as will be explained in more detail later.

Reference	Material	Q_m	Q_o	P_{th}	Phase Noise @ 1 kHz offset
[4]	SiO_2	2,000	5.5×10^6	250 μW	-60 dBc/Hz
[5]	SiO_2 (PSG)	7,200	2.8×10^6	N/A	-87 dBc/Hz
[6]	Si_3N_4	2,000	5.2×10^5	2 mW	-85 dBc/Hz
[5]	Si_3N_4	10,400	74,000	N/A	-102 dBc/Hz
[7]	Si	3,300	3.5×10^5	3.56 μW	N/A
[8]	Si	6,000	N/A	7.94 mW	-55.4 dBc/Hz
[9]	Si	376	42,000	~100 μW	~-40 dBc/Hz

Table 1: Summary of several RP-OMO devices and their performance. Silicon nitride OMO of [5] *achieves the lowest phase noise owing to its highest Q_m among all RP-OMOs, with an input optical power of 7.5 mW (P_{th} not explicitly measured). Silicon OMO in [7] posts dropped optical power of 3.56 μW.*

Early RP-OMO demonstrations used silica microtoroid resonators [1],[4] with ultra-high Q_o's in the order of 10^7, which led to remarkably low (~20 μW) optical threshold power. Although they exhibit low P_{th}, the phase noise in such oscillators has typically been poor, with best-to-date published phase noise value from a phospho-silicate glass (PSG) microring resonator of -87 dBc/Hz at a 1 kHz offset from a 18.6 MHz carrier [5]. An important aspect to note regarding silica OMO fabrication is that the microtoroid resonators require one-by-one laser annealing and PSG devices require high temperature (>1000 ºC) reflow to achieve such high Q_os.

More recently, silicon nitride microring resonators have shown the potential of RP-OMOs to be immune to flicker noise [6] and achieved promising low phase noise marks [5] for communications applications. Among single material OMOs, the work of [5] was able to achieve the lowest phase noise of -102 dBc/Hz at 1 kHz from its 74 MHz carrier by enhancing its Q_m over 10,400—a result of recognizing that mechanical Q_m has the strongest impact on phase noise, much more than the optical Q_o. Indeed, the silicon nitride OMO has posted a much lower Q_o of 74,000 (consequently, much higher P_{th}) than its silica counterparts.

Silicon OMOs also offer some promise especially in low power and high frequency applications. A microdisk OMO has achieved oscillation frequency beyond GHz with a low threshold at a dropped power below 4 μW [7]. However, the phase noise performance of this OMO is not reported so a measure of its frequency stability may be inferred from its Q_m=3,300. Although it is not driven by radiation pressure, an electrostatically actuated opto-acoustic oscillator comprised of silicon microring resonators in positive feedback with external electronic amplifiers has posted -80 dBc/Hz phase noise at 10 kHz offset from a 2.05 GHz carrier [10]. More recently, same resonator structure also realized a true RP-OMO [8] but with

a rather high phase noise value of -55.4 dBc/Hz at 1 kHz from its 175.3 MHz carrier despite operating at 80 K to attain Q_m=6,000. Other than the WGM devices, slot-type photonic crystal optomechanical cavities constructed in silicon have also shown parametric oscillations [9]. These devices offer high optomechanical coupling since the coupling is exponentially proportional to slot gaps between the beams which can be set to be on the order of wavelength of light (albeit, this needs electron beam lithography) whereas the optomechanical coupling scales with the radius of the cavity for WGM devices. Large optomechanical coupling provides an advantage to achieve low P_{th} and the work of [9] demonstrated an RP-OMO with P_{th} slightly above 100 μW. The measured Q_m=*376* is however very low and the posted phase noise is in the order of -40 dBc/Hz at a 1 kHz offset from a 65 MHz carrier.

Table 1 summarizes notable examples of the previous RP-OMOs. Note that there are many more optomechanical resonators using similar structures but they operate in the subthreshold regime (i.e. without oscillating) so they have not reported phase noise performance or threshold power.

1.3 Motivation

The ability to achieve self-sustained oscillation with no need for feedback electronics makes an RP-OMO compelling for on-chip applications where directed light energy, e.g., from a laser, is available to fuel the oscillation, such as Chip Scale Atomic Clocks (CSAC). Indeed, an RP-OMO can substantially reduce power consumption of a CSAC by replacing its power-hungry conventional quartz-based microwave synthesizer. The work of [5] gives a good discussion of this approach and it will be briefly described again here.

Atomic clocks generate a very stable frequency from the energy difference between the hyperfine states of an alkali metal atom, which is a constant of nature, and thereby, much more stable than a mechanical reference like quartz whose frequency is subject to long-term changes in mechanical dimensions and stress. Figure 1(a) presents the schematic of a chip scale one using Rubidium atoms for the frequency reference. Here, a cell containing Rb atoms in vapor state is interrogated by a 795 nm laser that corresponds to the wavelength for ^{87}Rb D1 transition, so the light is normally absorbed by the vapor cell. When the laser is modulated to generate sidebands apart by the 6.834682610 GHz hyperfine splitting frequency, it excites the atoms into a coherent dark state, where they become transparent to the interrogating laser light and no longer absorb it. A photodiode at the end of the vapor cell monitors the intensity of the laser light coming through the cell which gets maximized when the modulation frequency matches the hyperfine splitting frequency. A feedback circuit then locks the quartz based microwave oscillator to the hyperfine splitting frequency by controlling the frequency of the microwave oscillator so that the photodetector output current is maximized at the hyperfine peak. This microwave source consumes much power because it synthesizes the required ~3.4 GHz (half of the 6.834682610 GHz) signal from a 10 MHz voltage controlled crystal oscillator (VCXO) by using power hungry frequency division. Here, replacing the microwave source by a low power 3.4 GHz oscillator doesn't solve the problem since the actual clock output frequency near 10 MHz is desired, so some form of power-hungry

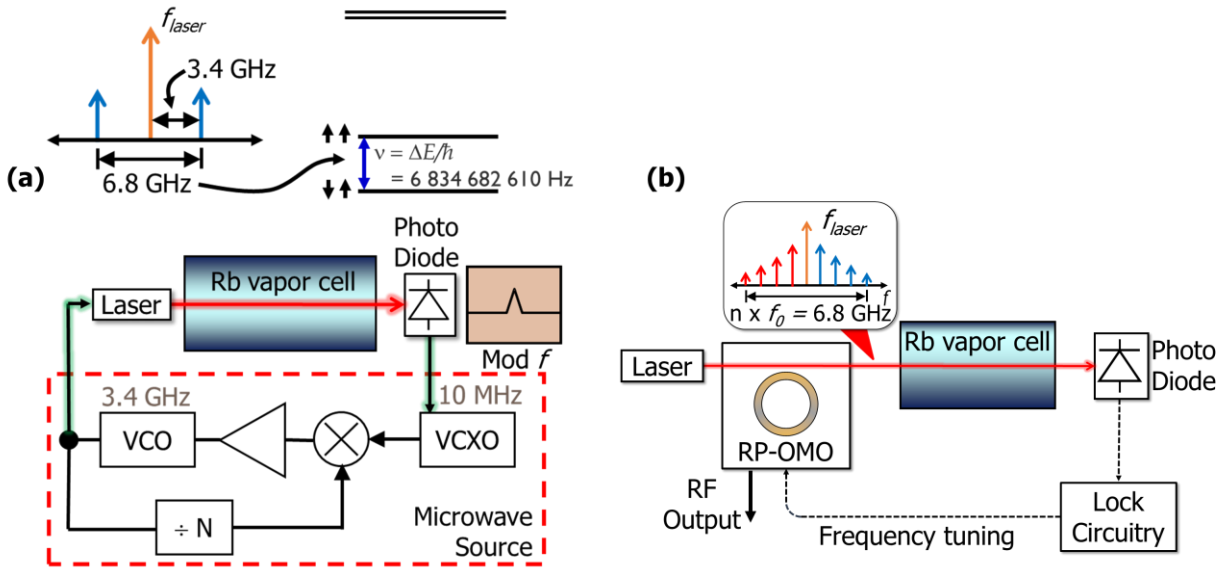

Figure 1: (a) Illustrates a Rb CSAC using a power-hungry microwave source implemented via a conventional synthesizer. The inset shows the excitation of hyperfine resonance via laser modulation, referred to as coherent population trapping (CPT). (b) Presents the targeted CSAC application where an RP-OMO's higher harmonic locks to a Rb vapor cell while the fundamental RP-OMO oscillation provides the clock output.

frequency division would still be required. It is the power consumption of the frequency divider that swamps the power consumption of other atomic clock parts, such as the micro-ovens needed to keep the Rb in vapor state, and the control electronics.

An RP-OMO could substantially reduce the CSAC power consumption by replacing its power-hungry microwave synthesizer. Figure 1(b) presents the targeted CSAC implementation using RP-OMO. Here, the RP-OMO modulates the pump laser at the mechanical resonance frequency and via non-linear mechanical and optical interaction at the higher harmonics as well. This efficient built-in harmonic generation would then allow exciting the hyperfine transition of the Rb cell with its harmonic at 3.4 GHz while providing a much lower standard frequency clock output without the need for power-hungry frequency division.

Although the Rb reference provides exceptional long term stability, the short term stability of the CSAC is still governed by its microwave source. In this regard, the RP-OMO output must have low phase noise for deployment as microwave oscillator in CSAC. Previous OMO experiments and modeling [5], [11], [12] suggest that the Q_m has the strongest effect on phase noise while the Q_o governs the loop gain of the system that ultimately sets the $P_{th.}$ This motivates a focus on achieving high Q_m while maintaining a reasonably high Q_o—a challenge in previous OMOs that had to trade-off Q_m and Q_m mainly because they use a single material to set both its Q_m and Q_o.

The work in this report presents a multi-material RP-OMO attaining simultaneous high Q_m and Q_o for use as a low-noise microwave oscillator for communications applications, e.g., chip-scale atomic clocks. The crux of this work is a mechanical circuit design that allows independent optimization of the Q_m and

Q_o of the composite resonant structure, thereby obviating the need to trade-off Q_m and Q_o that has hindered previous optomechanical resonator designs. Specifically, the multi-material OMO design combine a silicon nitride optical material with a lower mechanical loss polysilicon material that shares its energy to effectively boost the overall mechanical Q_m while maintaining the high Q_o provided by the silicon nitride cavity. The doped polysilicon structure and electrodes additionally allow tuning of the RP-OMO's oscillation frequency via DC voltage, enabling locking to an external reference very much needed for future deployment as a locked oscillator in the targeted CSAC application.

1.4 Outline

Chapter 2 begins with introducing the multi-material RP-OMO that combines a high Q_m polysilicon and a high Q_o silicon nitride ring to achieve simultaneous high Q_m and Q_o. It continues with the device design and explains the optomechanical operation, as well as the electrical input/output and frequency tuning enabled by the use of polysilicon material. Finally, it presents the mechanical Q-boosting concept that enables independent optimization of Q_m and Q_o.

Chapter 3 continues with the experimental results and presents the fabrication process for the multi-material RP-OMO. The measurement results demonstrate the highest measured Q_m and the lowest measured phase noise from an RP-OMO, as well as mechanical frequency tuning with applied voltage.

Finally, Chapter 4 concludes the report and gives a discussion on the impact of this work for the target application. It also discusses the opportunities for future enhancements and new applications that the multi-material RP-OMO might further enable.

Chapter 2

Multi-material Optomechanical Oscillator

Among single-material RP-OMOs, the work of [5] achieves the best-in-class phase noise for such devices of -102 dBc at a 1-kHz offset from a 74-MHz carrier by maximizing the mechanical Q_m of its optomechanical structure—a result of recognizing that mechanical Q_m has the strongest impact on phase noise, much more than optical Q_o. However, the performance of [5], although good, is still not sufficient, mainly because it uses a single material (silicon nitride) to set both its mechanical and optical Q's.

The RP-OMO described here (*cf*. Figure 2) circumvents this limitation by combining a nitride optical material with a lower mechanical loss polysilicon material that shares its energy to effectively boost the overall mechanical Q_m from 10,400 for a nitride device alone to 22,300. As a result of its high mechanical Q_m, the RP-OMO posts a phase noise of -114 dBc/Hz at 1 kHz offset from its 52-MHz carrier, which is 12 dB better than the previous state-of-the-art RP-OMO constructed of silicon nitride alone [5].

The doped polysilicon structure and electrodes additionally allow electrically coupled input/outputs, and tuning of the RP-OMO's oscillation frequency via DC voltage as indicated by V_p in Figure 2(a), enabling future deployment of the multi-material RP-OMO as a locked oscillator in the targeted CSAC application.

2.1 Device Structure and Operation

The Q-boosted RP-OMO, summarized in perspective-view and cross-section in Figure 2, comprises a high mechanical Q_m polysilicon inner ring physically attached at its outer edge to a concentric high optical Q_o (but comparatively low mechanical Q_m) silicon nitride ring. Spokes attached to the inner edges of the polysilicon ring extend radially inwards to a common central anchor and serve to support the entire multi-ring device in a completely balanced fashion, where inward forces along the spokes are met with equal and opposite ones, cancelling energy leakage from the spokes to the substrate as depicted in the finite element mode shape simulation in the inset of Figure 2(a). Polysilicon electrodes inside the ring overlap its inner edge to form capacitive gaps that then allow electrical interrogation and control (in addition to optical).

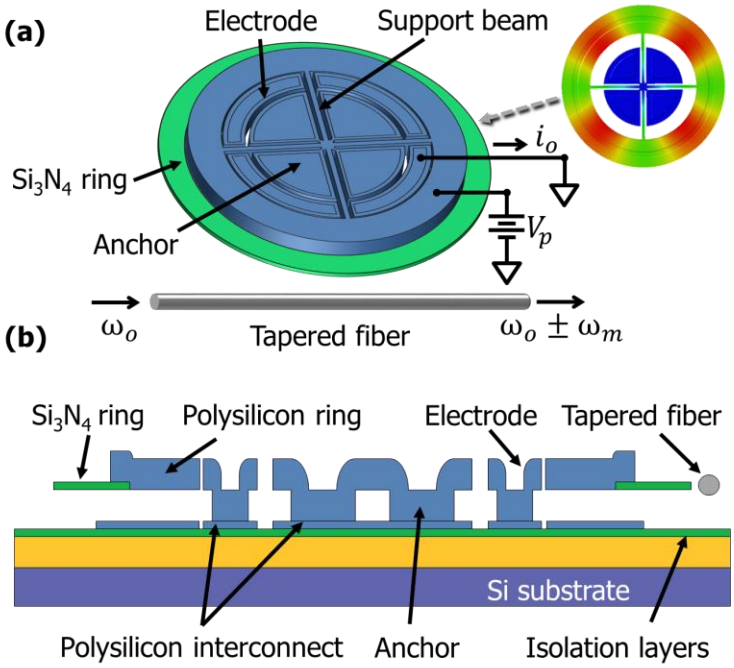

Figure 2: (a) Perspective-view and (b) cross-sectional schematics of the Q-boosted RP-OMO. Here, the polysilicon inner ring is mechanically coupled at its outer edge to a concentric high optical Q_o silicon nitride ring. A tapered fiber provides optical coupling, while polysilicon electrodes inside the ring enable frequency tuning and electrical input-output.

Both the polysilicon and silicon nitride rings supply vibrational energy to the composite structure in proportion to their effective masses, defined as $m_{eff} = 2U/\left(\omega_m^2 \cdot \Re(r)\right)$, where U is the total stored energy in the mechanical mode, ω_m the mechanical resonance frequency, and $\Re(r)$ the radial displacement amplitude at radius r. Because it is physically much larger, the polysilicon ring dominates the total effective mass m_{eff}, so its lateral dimensions govern to first order the *Q*-boosted OMO's mechanical resonance frequency (as will be seen). For a ring resonator without the support beams, the resonance frequency is defined by the transcendental equations [13]:

$$\begin{aligned}&[J_1(pr_i)\sigma - J_1(pr_i) + r_i p J_0(pr_i)] \times [Y_1(pr_o)\sigma - Y_1(pr_o) + r_o p Y_0(pr_o)] \\ &- [Y_1(pr_i)\sigma - Y_1(pr_i) + r_i p Y_0(pr_i)] \times [J_1(pr_o)\sigma - J_1(pr_o) + r_o p J_0(pr_o)] = 0\end{aligned} \tag{1}$$

$$f_m = \frac{p}{2\pi}\sqrt{\frac{E}{\rho(1-\sigma^2)}} \tag{2}$$

where r_i is inner ring radius, r_o outer ring radius, J's Bessel functions of the first kind, Y's Bessel functions of the second kind, ρ material density, σ Poisson's ratio, and E Young's modulus. The fundamental ("breathing") mode corresponding to $p = 1$ in Equations (1) and (2) couples most strongly to the optical resonator so the optical force excites this mode into oscillation.

2.1.1 Optical Operation and Optomechanical Oscillation

The silicon nitride outer ring enables optical input by accepting laser light from a waveguide—in this case, tapered fiber [14]—brought close enough to evanescently couple the light into to the silicon nitride ring. This ring then serves as a high-Q_o optical cavity that supports whispering gallery mode optical resonances, where the photons continuously circulate around the ring outer edges by repeated total internal reflection. Ideally, the light would circulate forever. In reality, of course, loss caused by scattering or coupling to nearby objects limits the time light can spend in the ring, which then limits the optical Q_o. Placement of the nitride ring at the outer edge of the structure avoids scattering from the polysilicon material or from coupling with the inner polysilicon electrodes, thereby maximizing the optical Q_o.

Once the ring structure vibrates (to be discussed in the next section), the ring motion appears as a modulation sideband spaced by the ring vibration frequency from the laser carrier. The same fiber that delivers the input light also provides output coupling from the silicon nitride ring back into the fiber. A photodiode can then demodulate the signal to isolate the mechanical resonance.

To incite self-sustained optomechanical oscillation, an input continues wave optical pump blue-detuned relative to the optical resonance of the silicon nitride ring couples into the ring. Enhanced by the Q_o, the circulating light generates a radiation pressure force that displaces the mechanical resonator which in turn shifts the optical resonance. As depicted in Figure 3(a), initially Brownian mechanical motion (strongest at the ring mechanical resonance frequency) modulates the optical pump field, which in turn generates a resonant radiation pressure force that modifies the mechanical dynamics. The coupling of the two degrees of freedom is described by the differential equations [2]:

$$\ddot{r}(t) + \Gamma_m \dot{r}(t) + \omega_m^2 r(t) = \frac{F_{rp}(t)}{m_{eff}} = \frac{1}{m_{eff}} \frac{2\pi n}{c} |A(t)|^2 \tag{3}$$

$$\dot{A}(t) + A(t)\left[\frac{\omega_o}{2Q_L} - i\Delta\omega + i\frac{\omega_o}{r_o} r(t)\right] = i\sqrt{\frac{\omega_o}{Q_e}|S|^2} \tag{4}$$

where $r(t)$ is the radial displacement of the mechanical resonator from equilibrium, Γ_m is the mechanical damping rate, ω_m is the mechanical resonance frequency, n is the effective refractive index for the optical mode, c is the speed of light, $A(t)$ the optical field circulating in the optical cavity, $\Delta\omega$ the detuning of laser from optical resonance frequency ω_o, $|S|^2$ the input optical power, Q_L the loaded quality factor of the optical resonance, Q_e the quality factor associated with coupling loss, and m_{eff} the mode dependent effective mass of the mechanical resonator.

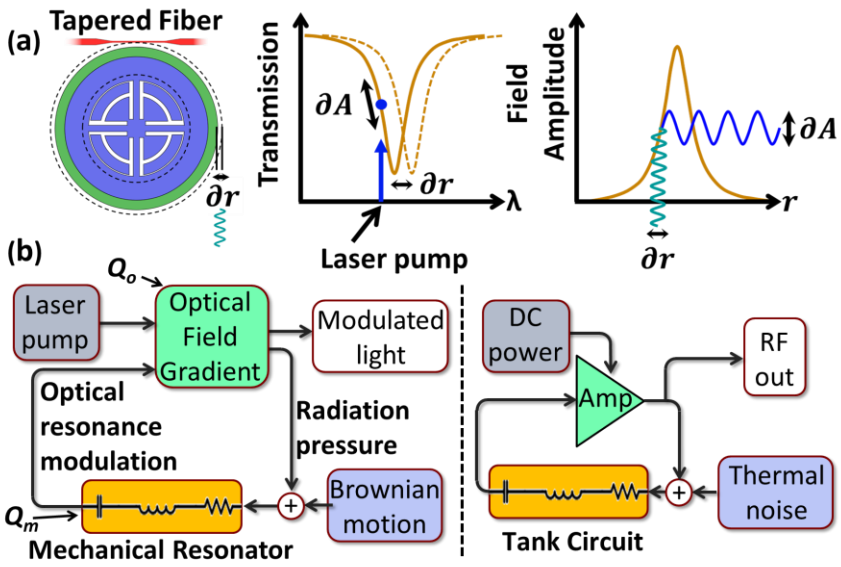

Figure 3: (a) Optomechanical oscillator dynamics: Radiation pressure from light in the cavity changes the radius which in turn changes the optical field, raising the radiation pressure, and so on, to generate a growing cycle. (b) System block diagrams comparing an RP-OMO with an electronic oscillator. The dynamics of the RP-OMO is analogous to an electronic oscillator where the optical field (with the high Q_o resonance) sets the gain and the mechanical resonator serves as the tank circuit feedback element.

When the laser intensity is strong enough, the displacement-to-radiation pressure force transfer function contributes sufficient gain to the optomechanical loop to achieve a loop gain greater than unity which then instigates regenerative oscillation growth. Effectively, the resonant radiation pressure force modifies the mechanical dynamics by acting as a negative mechanical damping that completely cancels out the intrinsic mechanical loss when the circulating optical power reaches a threshold value. From a feedback loop perspective, the optical pump power and Q_o sets the gain from the mechanical motion to the radiation pressure which gets positively fed back to the mechanical resonator as depicted in Figure 3(b), which further shows how the RP-OMO is in fact not so different from a conventional MEMS oscillator. Indeed, in both cases, the MEMS resonator in positive feedback serves as an ultra-high-Q bandpass biquad that accentuates the signal at resonance while suppressing noise off resonance. In this regard, high Q_m is of utmost importance if either system is to exhibit low close-to-carrier phase noise as predicted by the well-known Leeson's equation [15]:

$$L(f) \cong 10\log\left[\frac{2FkT}{P_{sig}}\left(1+\frac{1}{Q^2}\left(\frac{f_c}{2\Delta f}\right)^2\right)\right] \tag{5}$$

where $L(f)$ is the single side-band phase noise at an offset Δf from the carrier frequency f_c. F is a fitting parameter often termed as effective noise figure, k is the Boltzmann's constant, T is the absolute temperature, and P_{sig} is the output power of the oscillator having a tank-circuit element with quality factor Q, which is the mechanical quality factor for the case of an RP-OMO.

Meanwhile, the Q_o of the structure governs the optical field gradient that in turn sets the loop gain of the system, so must be at least high enough to initiate self-sustained oscillation. For maximum optical Q_o, the optical mode must not overlap with potential sources of optical loss, which dictates a minimum distance between the scatter-prone polysilicon-nitride attachment interface and the outer edge of the nitride ring. On the other hand, for maximum mechanical Q_m (as will be seen), the width of the nitride ring should be minimized relative to that of the polysilicon one. The nitride ring width thus serves as a design parameter through which RP-OMO performance can be optimized.

2.1.2 Electrical Operation and Voltage Controlled Frequency Tuning

Although the *Q*-boosted RP-OMO is a stand-alone oscillator that doesn't require external electronic circuitry for operation, it can also be driven electrically—a functionality not available in single nonconductive material RP-OMOs. Furthermore, it can also provide direct electrical output without the need for a photodetector to isolate the mechanical oscillation.

To enable electrical input/output, four polysilicon electrodes inside the polysilicon ring overlap its inner edge to form parallel plate capacitors that then realize capacitive-gap transducers. The electrodes anchor to underlying polysilicon interconnects that facilitate signal routing and connection to external electronic circuitry.

Obtaining an electrical output from the *Q*-boosted OMO entails applying a DC bias V_P across the conductive polysilicon ring and electrodes. When the radiation pressure drives the ring into oscillation, the ensuing motion modulates the DC-biased output capacitance C_{out} at the resonance frequency, generating displacement currents across this time-varying electrode-to-resonator gap:

$$i_o = V_P \frac{\partial C_{out}}{\partial t} = V_P \frac{\partial C_{out}}{\partial x}\frac{\partial x}{\partial t} \tag{6}$$

which can then serve as output signals proportional to displacement or velocity.

The electrodes additionally allow tuning of the RP-OMO's oscillation frequency (such as needed for CSAC application) via DC voltage. The applied voltage V_P generates a force from the resonator to the electrodes given by:

$$F_e = \frac{1}{2}\frac{\partial C}{\partial x} V_P^2 \tag{7}$$

where

$$\frac{\partial C}{\partial x} = \frac{C_o}{d_o}\left(1 - \frac{x}{d_o}\right)^{-2} \tag{8}$$

is to first order the change in electrode-to-resonator capacitance per unit radial displacement of the OMO, C_o is the static electrode-to-resonator overlap capacitance and d_o is the electrode-to-resonator gap spacing. For small displacements, the resonant force acting on the resonator becomes

$$F_e = V_P^2 \frac{C_o}{d_o^2} x \tag{9}$$

This force is proportional to and in phase with the resonator displacement, which identifies the term $V_P^2 \frac{C_o}{d_o^2}$ as a stiffness generated via electrical means [16]. Intuitively, the electrical force acts to enhance the displacement since it grows when the resonator gets close to electrode. Thus, the electrical stiffness subtracts from the mechanical stiffness, yielding a voltage dependent mechanical frequency given by

$$f_m = \frac{1}{2\pi}\sqrt{\frac{k_{eff}}{m_{eff}}} = \frac{1}{2\pi}\sqrt{\frac{k_m - k_e}{m_{eff}}} = f_{nom}\sqrt{1 - \frac{V_P^2 C_o}{k_m d_o^2}} \tag{10}$$

where f_{nom} is the nominal mechanical frequency under no DC voltage.

2.2 Mechanical *Q*-boosting

Again, the key to the phase noise performance obtained here is the high mechanical Q_m; and the key to the high Q_m is a concept introduced in [17] dubbed *Q*-boosting. *Q*-boosting is a mechanical circuit-based approach where a high-*Q* resonator raises the functional *Q* of a low-*Q* resonator in a mechanically coupled system by sharing its energy while adding relatively no loss [17]. In the multi-material RP-OMO, the polysilicon ring dominates the total effective mass m_{eff}, so the polysilicon ring contributes a larger portion of the total vibrational energy *U* in the system while introducing very little loss (because of its high mechanical Q_m). With energy added without additional loss, the composite structure then exhibits a much higher mechanical Q_m than otherwise provided by a silicon nitride-only ring.

Neglecting the loss at the nitride-polysilicon interface and possible change in the structure's anchor loss due to coupling of two materials, the functional mechanical $Q_{m,tot}$ of the composite structure can be expressed as:

$$Q_{m,tot} = 2\pi \frac{KE_{SiN} + KE_{pSi}}{E_{lost/cycle}} \tag{11}$$

where $E_{lost/cycle}$ is the total mechanical loss per cycle in the polysilicon and silicon nitride rings; and KE_{SiN} and KE_{pSi} are their respecitve kinetic energies, given by:

$$\begin{aligned} KE_{SiN} &= \frac{1}{2} \cdot m_{SiN} \cdot V_C^2 \\ KE_{pSi} &= \frac{1}{2} \cdot m_{pSi} \cdot V_C^2 \end{aligned} \tag{12}$$

where V_C denotes the radial velocity, m_{SiN} and m_{pSi} are effective lumped masses of the silicon nitride and polysilicon rings at the coupling location, respectively. Using (5) in (4) the functional $Q_{m,tot}$ simplifies to:

$$Q_{m,tot} = Q_{m,pSi}\frac{1+\frac{m_{SiN}}{m_{pSi}}}{1+\frac{m_{SiN}}{m_{pSi}}\cdot\frac{Q_{m,pSi}}{Q_{m,SiN}}} \tag{13}$$

which shows that the total $Q_{m,tot}$ of the RP-OMO structure depends on the Q_m and effective mass of both structures.

Chapter 3

Experimental Results

3.1 Fabrication and Geometric Design

Multi-material RP-OMOs were surface micromachined on a six-inch silicon substrate. Figure 4(a) presents a colorized Scanning Electron Micrograph (SEM) of a fabricated multi-material RP-OMO and Figure 4(b) illustrates the fabrication process. Here, low-temperature oxide (LTO) and silicon nitride layers provide electrical isolation between the silicon substrate and the subsequently deposited polysilicon layer. The doped polysilicon mechanical structure and inner capacitive gap electrodes are anchored and electrically connected to a thin layer of conductive polysilicon patterned on the substrate to serve as interconnects that facilitate electrical interrogation and read-out. The electrodes additionally allow tuning of the RP-OMO's oscillation frequency (such as needed for CSAC application) via well-known voltage-controllable electrical stiffness [16].

Table 2 presents the *Q*-boosted OMO and a polysilicon-only ring design with their measured resonance frequencies. Here, the *Q*-boosted OMO and the polysilicon-only ring have the same polysilicon ring dimensions. Measured resonance frequencies of both structures are in close agreement with the calculated values for the polysilicon ring geometry, confirming that the polysilicon structure governs to first order the *Q*-boosted OMO's mechanical resonance frequency.

	Polysilicon-only ring	*Q*-boosted OMO
Polysilicon r_i	20 μm	20 μm
Polysilicon r_o	30 μm	30 μm
Si_3N_4 width	-	6.5 μm
Calculated polysilicon ring frequency	52.06 MHz	52.06 MHz
Measured frequency	52.69 MHz	52.00 MHz

Table 2: Q-boosted OMO design and its polysilicon-only counterpart for comparison. The polysilicon ring geometry governs the entire Q-boosted OMO's resonance frequency as indicated by the close agreement between the calculated and measured values.

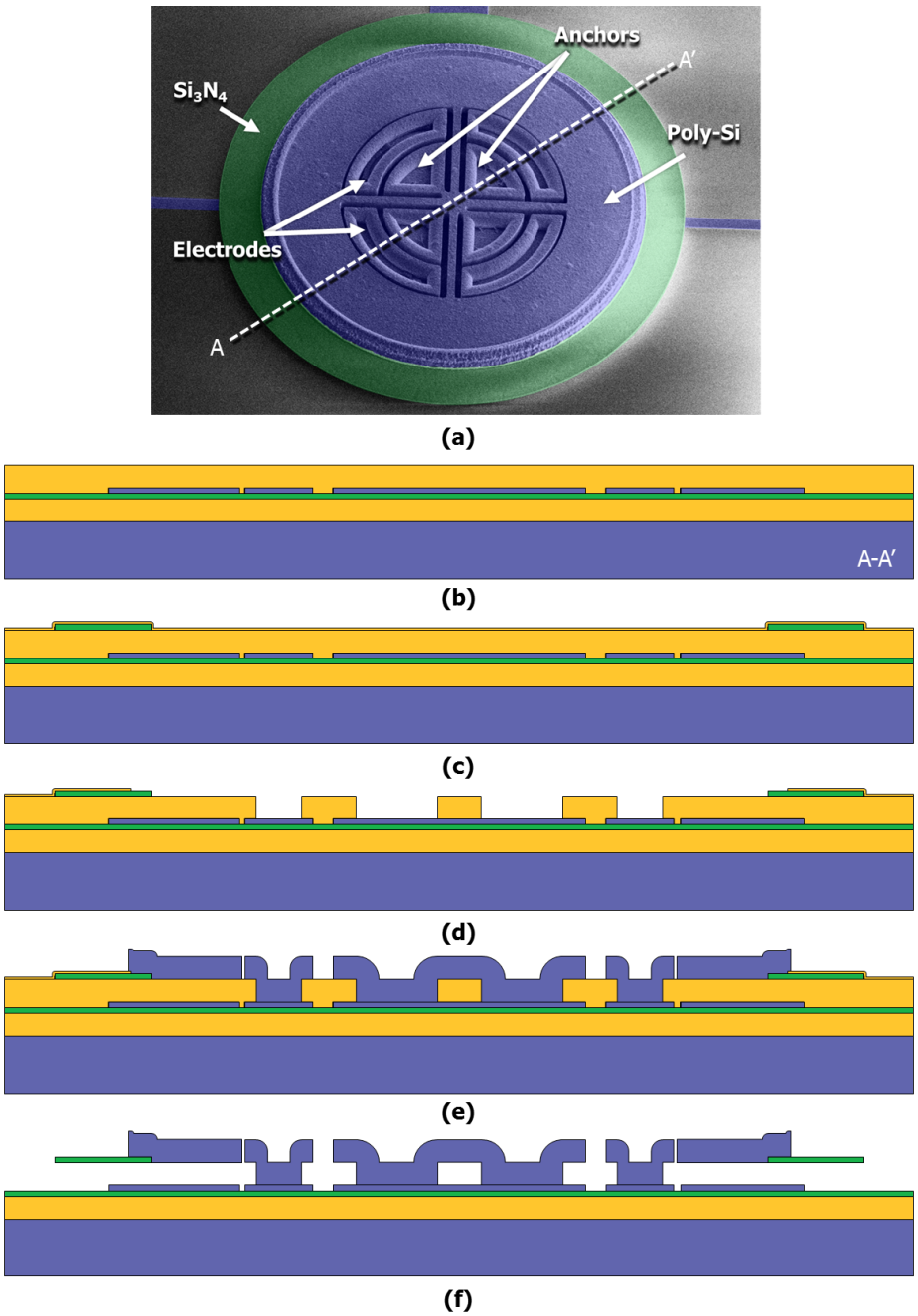

Figure 4: (a) Colorized SEM image of the fabricated multi-material Q-boosted RP-OMO. (b)-(e) Summary of the fabrication process flow. (b) Low-temperature $Si0_2$ (LTO) and Si_3N_4 layers are deposited for electrical isolation and etch stop followed by polysilicon interconnect deposition and etch. Another LTO layer is deposited and CMP'ed to a final thickness of 2 μm, leaving a planar surface for the Si_3N_4. (c) The optical cavity is formed by patterning a 400 nm Si_3N_4 film and protected during subsequent etches by a thin layer of LTO. (d) Anchors are defined by etching $Si0_2$. (e) 2 μm of polysilicon is deposited and etched to define the polysilicon ring structure and the electrodes. (f) Finally, devices are released in 49% hydrofluoric acid.

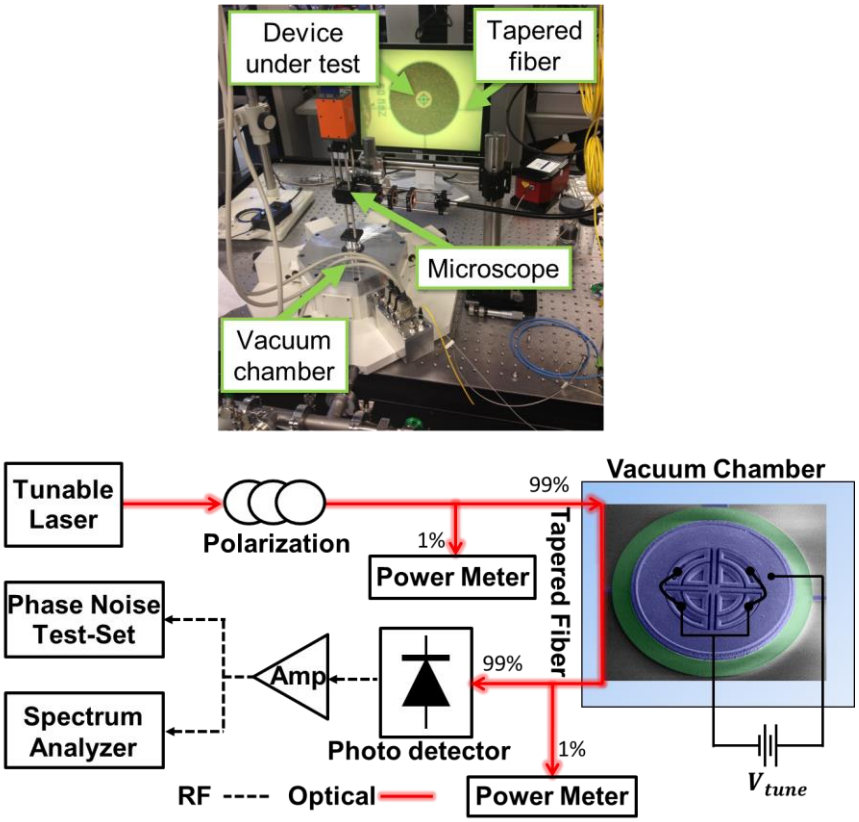

Figure 5: Experimental measurement setup. The RP-OMO is characterized in a custom-built vacuum chamber as described in [5]. *An Agilent E5505A phase noise test system is used for phase noise measurements.*

3.2 Experimental Setup and Measurements

Q-boosted RP-OMO measurements used the custom-built vacuum system of [5] in which a sealed probe station provides easy access to device electrodes, and nano-positioning piezo stages provide precise control of optical coupling. Figure 5 shows the experimental setup used to characterize the RP-OMO where a Newfocus TLB-6728 tunable laser serves as the pump laser and provides accurate detuning from the RP-OMO optical resonance. The RF output from the photodiode+amplifier chain feeds an Agilent N9030A spectrum analyzer and an E5505A phase noise test system.

Measurement of Brownian noise shown in Figure 6(a) reveals a multi-material RP-OMO boosted Q_m of 22,300, which is more than 2× higher than demonstrated in a previous silicon nitride RP-OMO [5]. To gauge the degree to which Equation (13) matches the measured $Q_{m,tot}$ requires knowledge of the $Q_{m,pSi}$ of a spoke-supported polysilicon ring and the $Q_{m,SiN}$ of an unsupported nitride ring. The former is readily measured to be 40,900 (with an s21 measurement using an Agilent E5071B RF network analyzer) on the polysilicon spoke-supported ring (*cf*. Figure 6(b)) that has exact same geometry as the *Q*-boosted OMO but without any silicon nitride attached. The Q_m of an unsupported nitride ring, on the other hand, is much more elusive, since any real fabricated nitride ring does have supports, so suffers from anchor loss not present in an unsupported (levitated) ring. One reasonable approximation, however, might be the

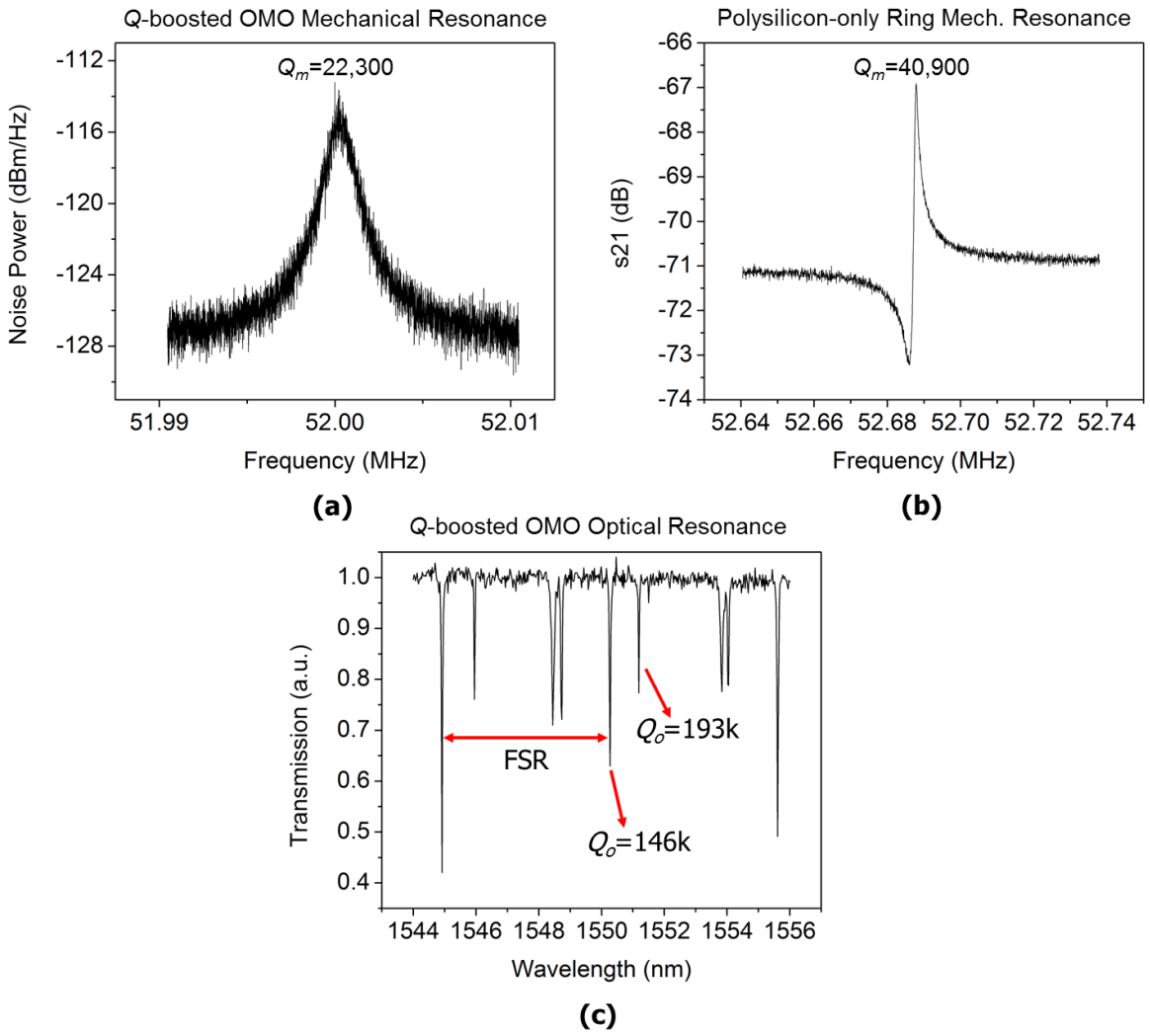

Figure 6: (a) Measured Brownian motion of the Q-boosted RP-OMO from which Q_m=22,300 is extracted. (b) Electrically measured insertion loss of the polysilicon-only ring exhibiting a high Q_m of 40,900. (c) Q-boosted RP-OMO's measured optical resonances with highest Q_o=193,000.

highest Q_m of 10,400 measured among several fabricated spoke supported 1st radial-contour mode silicon nitride rings [5] at the frequency of interest. With the above Q_m values and 1.61 ng nitride and 7.76 ng polysilicon effective masses calculated from the device dimensions given in Table 2, Equation (13) predicts a $Q_{m,tot}$ of 27,195 for the composite RP-OMO which is reasonably close to the measured value of 22,300.

The multi-material OMO design also attains high Q_o >190,000 as the optical transmission spectrum of Figure 6(c) presents. This is on par with previous silicon nitride ring designs [5] [6], indicating that the multi-material design have little or no effect on the optical properties of the high Q_o silicon nitride ring.

Figure 8(a) and (b) present the RP-OMO's output spectra under several tuning voltages and measured plots gauging oscillating RP-OMO frequency versus tuning voltage, where a relatively large 440 nm electrode-to-resonator gap spacing still allows a 3 ppm/V frequency shift suitable for locking to the Rb

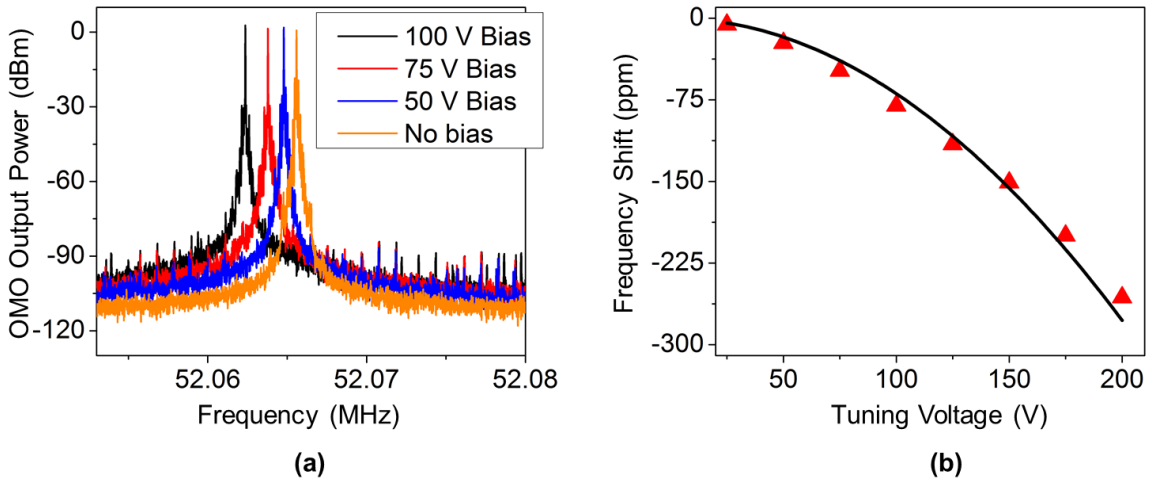

Figure 8: (a) Q-boosted OMO output spectra under several different applied tuning voltages showing the voltage controlled frequency tuning. (b) Measured frequency shift (red data points) via curve-fitting (black line) indicates a 440 nm resonator-to-electrode gap spacing.

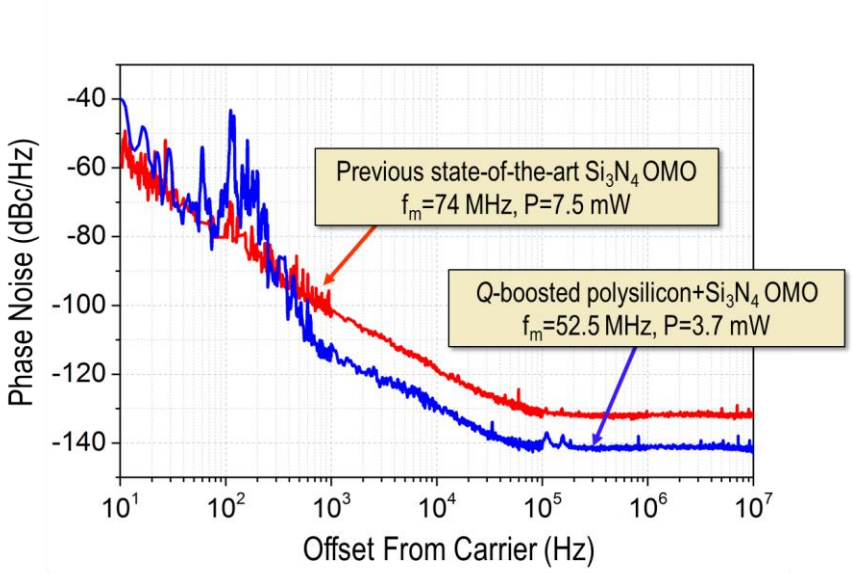

Figure 7: Phase noise spectra of the Q-boosted RP-OMO compared to the previous best silicon nitride only RP-OMO [5]. *As expected, the enhanced Q_m lowers the phase noise, achieving a 12 dB improvement at 1 kHz offset, while consuming only 3.7 mW.*

vapor cell in a CSAC.

Fig. 6 presents the measured phase noise (blue) for the *Q*-boosted RP-OMO of -114 dBc/Hz at 1 kHz offset and -142 dBc/Hz at far-from-carrier offsets from its 52-MHz carrier, which is more than 12 dB better than the previous state of the art RP-OMO (red) constructed of silicon nitride alone [5], despite the use of an input laser power of only 3.7 mW—more than 2× smaller than that of the previous state-of-the-art [5].

Chapter 4

Conclusions

A multi-material RP-OMO structure has been shown to boost the Q_m of a silicon nitride RP-OMO by more than 2× toward realization of the simultaneous high Q_m >22,000 and Q_o >190,000 needed to maximize RP-OMO performance. This is the highest measured Q_m among all the RP-OMOs to the best of our knowledge. The design is shown to have little or no effect on the optical properties of the high Q_o silicon nitride ring cavity, allowing retention of high Q_o despite the introduction of a scatter-prone material interface in the vicinity of the optical resonance. While polysilicon is chosen for its high Q_m in the RP-OMO of this work, the design is applicable to any material of choice as long as it can be integrated with another high Q_o material of choice.

The Q-boosted RP-OMO bests the previous state-of-the-art by reducing the phase noise at 1 kHz offset from the carrier by a measured 12 dB that matches the prediction of Equation (5) with the improved Q_m. The measured phase noise of -114 dBc/Hz at 1 kHz offset and -142 dBc/Hz at far-from-carrier offsets, when normalized to GSM's 13 MHz for comparison, correspond to -126 dBc/Hz and -154 dBc/Hz, respectively. This satisfies GSM reference oscillator phase noise requirement at far-from-carrier offsets and it is only 4 dB off at 1 kHz offset, which makes the RP-OMO a good candidate for communications applications.

The boosted Q_m also helps operating with a lower power. The use of an input laser power of only 3.7 mW is already more than 2× smaller than that of the previous state-of-the-art and makes the multi-material OMO an ideal candidate to replace the power hungry microwave oscillator (consuming ~100 mW) of a CSAC. This would substantially lower the total (~150 mW) CSAC power consumption and open the potential of using atomic clocks in portable devices.

The use of high Q_m doped polysilicon as one of the materials further enables electrical interrogation and readout of the RP-OMO, as well as an electrical stiffness-based voltage controlled frequency tuning very much needed for locking in the target low-power CSAC application. Although the demonstrated 3 ppm/V frequency shift is suitable for locking to the Rb vapor cell in a CSAC, a reduced electrode-to-resonator gap spacing would easily allow much larger frequency shifts. The first demonstration here defines the polysilicon resonator and electrodes in one lithography step, yielding a relatively large 440 nm electrode-to-resonator gap spacing. Conventional capacitive-gap MEMS devices can easily achieve gap spacing below 100 nm defined by a sidewall sacrificial layer deposition, which can also be used in a future RP-OMO generation.

The added electromechanical coupling allows integration of cavity optomechanics with conventional MEMS, in which the high-Q mechanical resonator is coupled to both an electrical circuit as well as an optical cavity. This integrated electro-optomechanical system can enable further applications where optical signals modify electrical properties and vice versa.

Bibliography

[1] H. Rokhsari, T. J. Kippenberg, T. Carmon, and K. J. Vahala, “Radiation-pressure-driven micro-mechanical oscillator,” *Opt. Express*, vol. 13, no. 14, pp. 5293–5301, 2005.

[2] M. Hossein-Zadeh and K. J. Vahala, “An optomechanical oscillator on a silicon chip,” *IEEE J. Sel. Top. Quantum Electron.*, vol. 16, no. 1, pp. 276–287, 2010.

[3] F. Liu, S. Alaie, Z. C. Leseman, and M. Hossein-Zadeh, “Sub-pg mass sensing and measurement with an optomechanical oscillator.,” *Opt. Express*, vol. 21, no. 17, pp. 19555–67, 2013.

[4] M. Hossein-Zadeh, H. Rokhsari, A. Hajimiri, and K. Vahala, “Characterization of a radiation-pressure-driven micromechanical oscillator,” *Phys. Rev. A*, vol. 74, no. 2, pp. 405–408, 2007.

[5] T. O. Rocheleau, A. J. Grine, K. E. Grutter, R. A. Schneider, N. Quack, M. C. Wu, and C. T.-C. Nguyen, “Enhancement of mechanical Q for low phase noise optomechanical oscillators,” *Proceedings, 2013 IEEE 26th International Conference on Micro Electro Mechanical Systems (MEMS)*, 2013, pp. 118–121.

[6] S. Tallur, S. Sridaran, and S. A. Bhave, “A Silicon Nitride Optomechanical Oscillator With Zero Flicker Noise,” *Proceedings, 2012 IEEE 25th Int. Conf. Micro Electro Mech. Syst.*, pp. 19–22, 2012.

[7] W. C. Jiang, X. Lu, J. Zhang, and Q. Lin, “High-frequency silicon optomechanical oscillator with an ultralow threshold,” *Opt. Express*, vol. 20, no. 14, pp. 15991–15996, Jul. 2012.

[8] M. J. Storey, S. Tallur, and S. A. Bhave, “Radiation-pressure enhanced opto-acoustic oscillator,” *Proceedings, 2014 IEEE 27th International Conference on Micro Electro Mechanical Systems (MEMS)*, 2014, pp. 1209–1212.

[9] J. Zheng, Y. Li, M. Sirin Aras, A. Stein, K. L. Shepard, and C. Wei Wong, “Parametric optomechanical oscillations in two-dimensional slot-type high-Q photonic crystal cavities,” *Appl. Phys. Lett.*, vol. 100, no. 21, p. 211908, 2012.

[10] S. Tallur and S. A. Bhave, “Monolithic 2GHz Electrostatically Actuated MEMS Oscillator with Opto-mechanical Frequency Multiplier,” *Proceedings, the 17th International Conference on Solid-State Sensors, Actuators and Microsystems (Transducers'13)*, 2013, pp. 1472–1475.

[11] A. J. Grine, K. E. Grutter, T. O. Rocheleau, N. Quack, T. Beyazoglu, Z. Zheng, I. Jutla, C. T.-C. Nguyen, and M. C. Wu, “Phase Noise Spectrum and Carrier Power Modeling of High Performance Optomechanical Oscillators,” *Proceedings, Conference on Lasers and Electro-Optics (CLEO)*, 2013, p. 1,2.

[12] S. Tallur, S. Sridaran, S. A. Bhave, and T. Carmon, “Phase noise modeling of opto-mechanical oscillators,” in *Proceedings, Proceedings, 2010 IEEE Int. Freq. Control Symp. FCS 2010*, pp. 268–272, 2010.

[13] S.-S. Li, Y.-W. Lin, Y. Xie, Z. Ren, and C. T.-C. Nguyen, “Micromechanical ‘Hollow-Disk’ Ring Resonators,” *Proceedings, 17th Int. IEEE Micro Electro Mechanical Systems Conf.*, 2004, pp. 821–824.

[14] J. C. Knight, G. Cheung, F. Jacques, and T. a. Birks, "Phase-matched excitation of whispering-gallery-mode resonances by a fiber taper," *Opt. Lett.*, vol. 22, no. 15, p. 1129, Aug. 1997.

[15] D. B. Leeson, "A simple model of feedback oscillator noise spectrum," *Proc. IEEE*, vol. 54, no. 2, pp. 329–330, 1966.

[16] H. C. Nathanson, W. E. Newell, R. A. Wickstrom, and J. R. Davis, "The Resonant Gate Transistor," *IEEE Trans. Electron Devices*, vol. 14, no. 3, pp. 117–133, 1967.

[17] Y.-W. Lin, L.-W. Hung, S.-S. Li, Z. Ren, and C. T.-C. Nguyen, "Quality factor boosting via mechanically-coupled arraying," *Proceedings, the 14th Int. Conf. on Solid-State Sensors & Actuators (Transducers'07)*, 2007, pp. 2453–2456.